High-Temperature Molten Salts for Use in Solar Thermal Energy Systems

R. T. Coyle, R. J. Copeland, R. W. Burrows and R. M. Goggin

Solar Energy Research Institute
Golden, Colorado, USA

ABSTRACT

Research is being conducted with advanced molten salts (hydroxides, carbonates and chlorides) for solar thermal applications. These salts may be used in the receiver working fluid and in thermal energy storage. Potential applications include electric power production, fuel and chemical production, and high-temperature process heat. Molten salts can store sensible heat at temperatures up to 1100°C in a thermocline system. Salt corrosion of the insulating and containment materials is a major area of concern, and current results of research on corrosion in molten hydroxide and molten carbonates are described.

INTRODUCTION

Molten salts have been used for many years in the chemicals and metals industries. Common applications include removing heat from exothermic reactors and providing heat to processing equipment such as evaporators and concentrators (Watt and Kerridge, 1979). They have also found widespread use as a bath medium for heat treating metals (Foreman, 1980). Recently, interest in molten nitrate salts has heightened because of their proposed use in solar energy systems (Tallerico, 1979). Because the molten nitrate salts will decompose above 600°C, new salts have been identified for applications up to 1100°C (Copeland, Leach, and Stern 1982). These applications include solar thermal process heat, electric power and fuels production (e.g., hydrogen from solar energy and water). The candidate molten salts include carbonates, chlorides and hydroxides and are to be used as the fluid for heat transfer and thermal energy storage. This paper describes the solar thermal system in which they will be used and the current research using carbonate and hydroxide salts that has been done in identifying suitable materials to contain the salts.

SOLAR ENERGY SYSTEMS

Central-Receiver System

Solar-thermal central-receiver systems are being developed for electric power and other applications. This type of system is exemplified by the Solar One plant in Barstow, California, which is illustrated in Figure 1. It consists of a heliostat field, a receiver, a thermal energy storage system

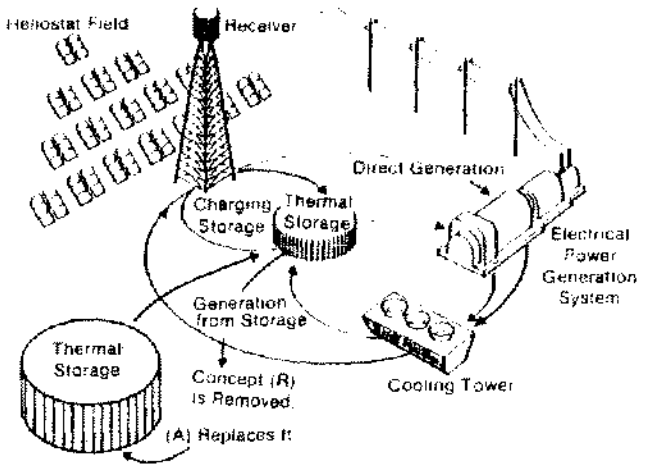

Figure 1. Illustration of a Solar Central Receiver System for Generating Electricity.

and an electric power generation system. In operation, solar radiation strikes a field of heliostats (computer-driven mirror reflectors) that focus the radiation onto a central receiver. There the energy is absorbed by a heat-transfer fluid (water at the Barstow plant) that is then diverted to the thermal energy storage system. The storage system serves two purposes, to extend the time of operation beyond the hours where there is adequate insolation and to buffer the electrical generation equipment from the intermittent nature of the radiant flux that is inherent in a solar energy source. By using a secondary water and steam heat-

transfer loop, the thermal energy storage system converts water to superheated steam, which is then used to drive the electric generating turbines of a steam Rankine cycle.

The energy from the receiver may also be used to generate electricity directly. In this case, if the primary heat-transfer fluid is not water, a secondary heat exchange loop is necessary to generate the steam. A convenient system concept is to have one fluid serve as the heat-transfer fluid as well as the storage medium. Molten nitrate salt is such a heat-transfer fluid that can also be used for thermal energy storage up to 600°C (Battleson et al., 1980, Mar and Carling, 1980). For higher operating temperatures, advanced systems using other molten salts show promise of being cost-effective (Copeland, 1982; Copeland, Leach and Stern, 1982).

Electric Power Generation Application

A concept for an advanced, high-temperature molten salt system for generating electric power is presented in Figure 2. In this concept an advanced molten salt receiver collects solar thermal energy at temperatures as high as 1100°C. Thermal energy is then stored using the salt as a medium in an internally insulated tank with a thermocline. Heat is transferred to pressurized air in a direct-contact, molten salt heat exchanger, and a combined cycle system (Brayton/Steam-Rankine) generates the electric power.

A conceptual tank design for storage at 1100°C that uses the salt itself as inexpensive insulation in the sides of the tank is shown in Figure 3. Although the conductivity of the salt is low, a rigid internal structure is needed to prevent natural convection in the salt. This design uses a stainless steel honeycomb with cell dimensions of approximately 0.63 cm (0.25 in.) for the rigid structure of the insulation. For this type of insulation the liquid level in the tank must be maintained nearly constant to prevent the 1100°C salt from flowing into the honeycomb and contacting the carbon steel outer tank structure. Therefore, a thermocline tank design that maintains a constant liquid level is most appropriate. Additionally, since the radiation exchange between the hot and cold layers of the thermocline can be significant, a raft (shown in the figure) is included to reduce this heat transfer.

The receiver, shown schematically in Figure 4, uses direct absorption of the concentrated solar radiation in the molten salt. The salt is blackened with a suitable transition metal oxide (e.g., cobalt oxide) to promote absorption. Experiments with molten nitrate salts show that this direct absorption concept is functional (Brumleve, 1978). The vapor pressures of the candidate salts are sufficiently low so that the vapor can be contained within the receiver cavity with minimal losses.

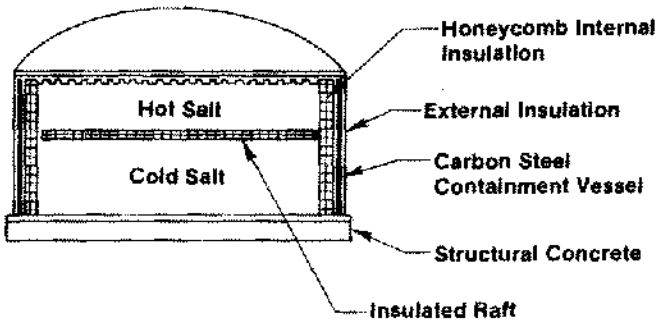

Figure 3. Illustration of a High-Temperature Molten Salt Storage Tank Concept.

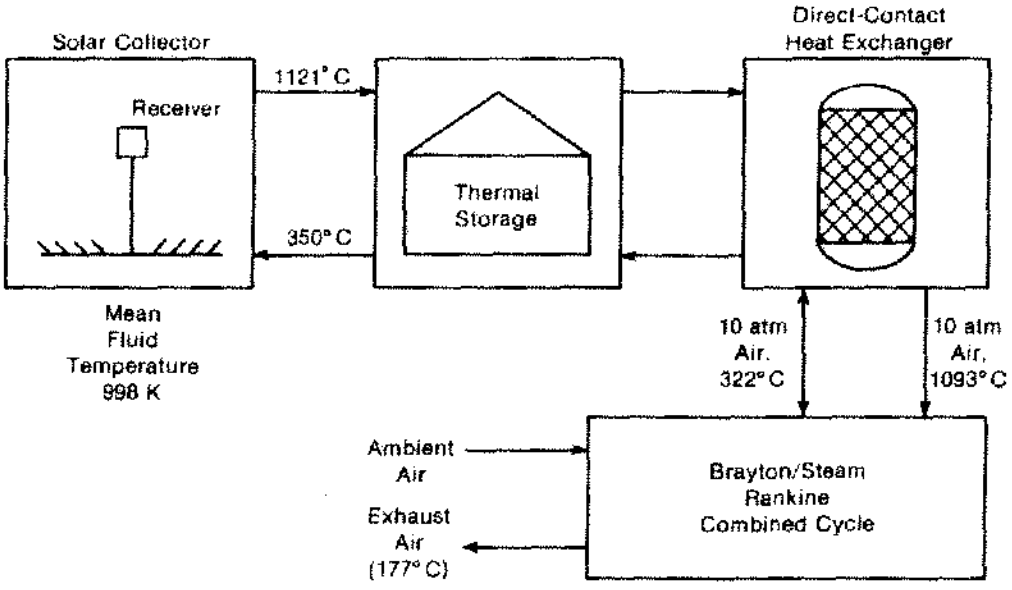

Figure 2. Concept for an Electric Power Generation System with a High-Temperature Molten Salt Storage Tank.

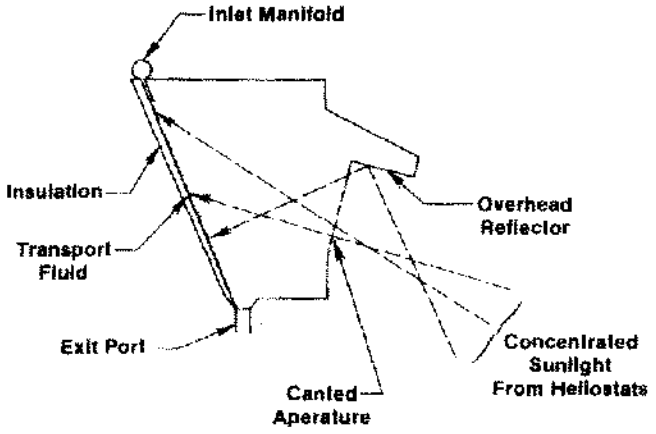

Figure 4. Illustration of a Direct Absorption Receiver Concept.

Several salts can be used as the thermal storage media and also as the receiver working fluid. Sodium hydroxide (NaOH), carbonates and chlorides are all inexpensive and stable up to 1100°C. Because of the high operating temperatures that they permit, all three of these molten salts can be used in systems that are less costly than the lower temperature molten nitrate system.

We compared systems containing high-temperature molten salt storage to other central-receiver power generation systems, and Figure 5 presents the results. The data for all but the high-temperature molten salt system were received from Sandia National Laboratory (Battleson, 1980). The same data base for costs was used for the high-temperature molten salt system and other systems. Although these results are preliminary, the advanced molten salt system shows a high potential.

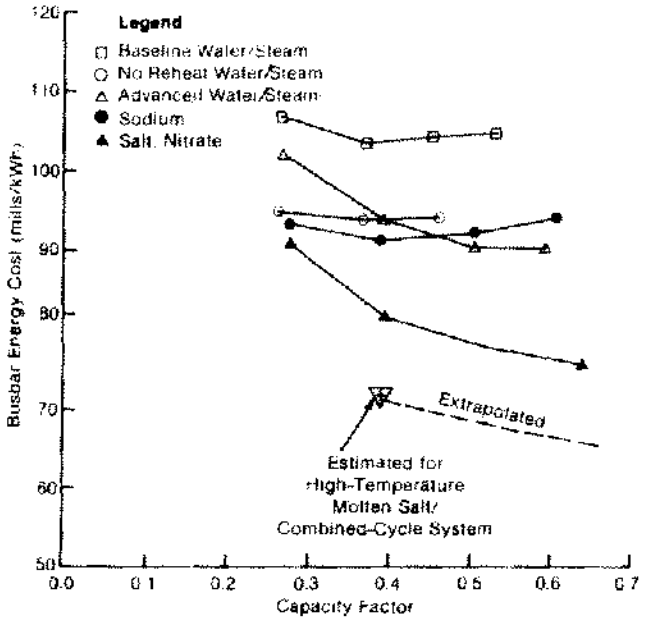

Figure 5. Solar Central Receiver Busbar Electricity Cost as a Function of Capacity Factor.

CORROSION OF MATERIALS IN MOLTEN SALTS

Experimental Techniques for Corrosion

An apparatus for measuring the corrosion rate of candidate containment materials is shown schematically in Figure 6. Two Lindberg crucible furnaces each contain three of these 99.8% pure aluminum oxide crucibles to hold the molten salt. The crucibles are capped with a water-cooled plate through which are mounted thermocouples to monitor the crucible temperature and gas purge tubes to maintain the desired atmosphere above the molten salt. Mass flow controllers maintain a constant flow of purge gas to the crucibles, and gas flow meters distribute gas equally into the three crucibles of each furnace. The gas control sys-

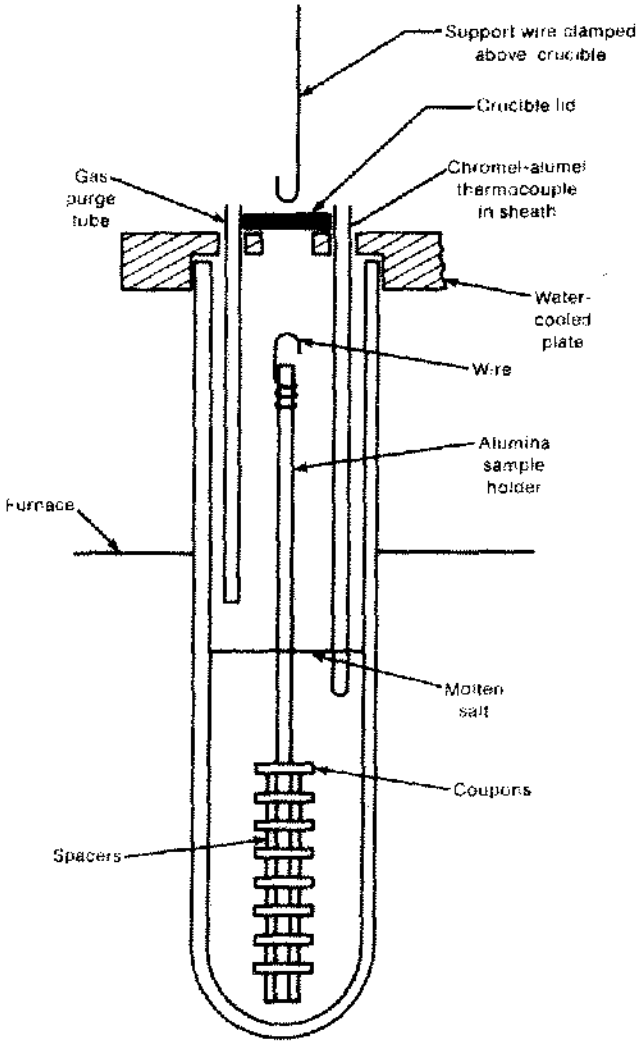

Figure 6. Schematic of a Crucible for Conducting Molten Salt Corrosion Experiments.

tem allows two different gases to be mixed in the desired ratio to achieve suitable composition for the purge gas. The temperatures in the crucibles were continuously monitored by chromel-alumel thermocouples connected to a Fluke scanning digital thermometer system that includes a printer.

Test coupons of ceramic and alloy candidates were cut to 1.3 × 1.9 cm and were typically about 0.3 cm thick. A typical coupon is shown before and after testing in Figure 7. Holes of about 0.4 cm diameter were made in the coupons so that we could mount them on a 99.8% aluminum oxide sample holder with 99.8% aluminum oxide spacers. We lowered the sample holder into the crucible using a support wire that was attached to the ceramic on one end and clamped on the other end about 50 cm above the water-cooled plate. We slowly lowered them into the crucible by unclamping, lowering a short distance, then clamping and waiting for the sample holder to rise in temperature.

All of the experiments in this work were done at 900°C. Each crucible contained about 300 cc of molten salt that filled the crucible to a depth of about 19 cm. All of the samples were immersed in the salt, and the temperature gradient in the molten salt was about 4°C.

Molten Salt Chemistry

Several studies of the influence of molten salt chemistry on the corrosion of materials have been published (Rapp and Goto, 1980; Smith, 1956; Littlewood, 1962; Ingram and Janz, 1965). The acid-base character of the molten salt as well as its oxidation potential provide valuable insight for understanding the dissolution of materials in these fluids. For carbonate salts the dissociation reaction of the carbonate ion can be written (Ingram and Janz, 1965; Inman and Wrench, 1966).

$$CO_3^{2-} \rightleftharpoons O^{2-} + CO_2,$$

where CO_3^{2-} acts as a base in the Lux-Flood (Lux, 1939; Flood, Forland, and Motzfeld, 1952) acid-base scheme by supplying the oxide ion, and CO_2 is the conjugate acid. The oxide ion is also the controlling factor in the acid-base behavior of neutral salts such as chlorides because of oxygen impurities present in the chlorides (Littlewood, 1962).

This acid-base behavior as well as the oxidation-reduction potential for a material is commonly represented on phase stability diagrams such as the one shown in Figure 8 for Al_2O_3 at 1200 K in Na_2SO_4 (ℓ) (Rapp and Goto, 1980). Similar diagrams for carbonates and hydroxides can be constructed from appropriate thermochemical data where SO_3 is replaced by CO_2 and H_2O, respectively, for the carbonates and hydroxides. The more acidic salt condition corresponds to positive values for log P_{SO_3} and more oxidizing conditions for the melt are at the more positive values of log P_{O_2}. At low oxygen pressures, Al_2S_3 becomes stable; for carbonate and hydroxide molten salts Al metal would be formed under low P_{O_2} reducing conditions. For oxide ceramic materials, such as Al_2O_3, the principal factor in judging corrosion reactions in molten salts is the acid-base value of the salt as seen in the diagram. The acid-base value is also important for alloys oxidized by the molten salt, because dissolution of the oxide would leave the alloy susceptible to further oxidation.

Al^{+3} ions as $Al_2(SO_4)_3$ become the stable phase at the most positive values of log P_{SO_3} in Figure 8. At values of log P_{SO_3} in the vicinity of zero, α-Al_2O_3 is the stable phase but in equilibrium with a substantial concentration of Al^{+3} in the molten Na_2SO_4. Thus, significant corrosion of the α-Al_2O_3 must occur to establish this concentration. At log P_{SO_3} values in the vicinity of -10, the Al^{+3} ions are complexed to form an AlO_2^- molecule that is insoluble in the presence of alkali ions and forms a sodium aluminate phase. The potential for forming complex molecules under highly basic conditions can lead to increased corrosion in a system that does not form an insoluble compound such as the $NaAlO_2$ in this system.

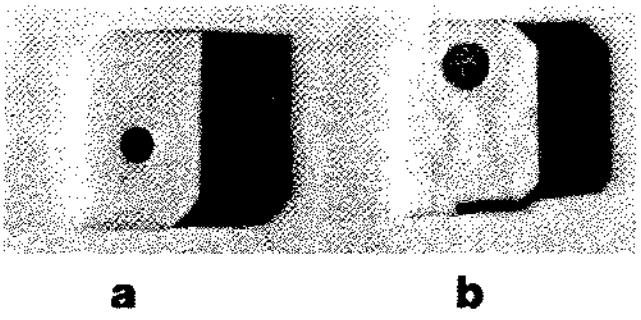

Figure 7. Al_2O_3, 99.8%, before and after Exposure to Hydroxide at 900°C for 48 Hours.

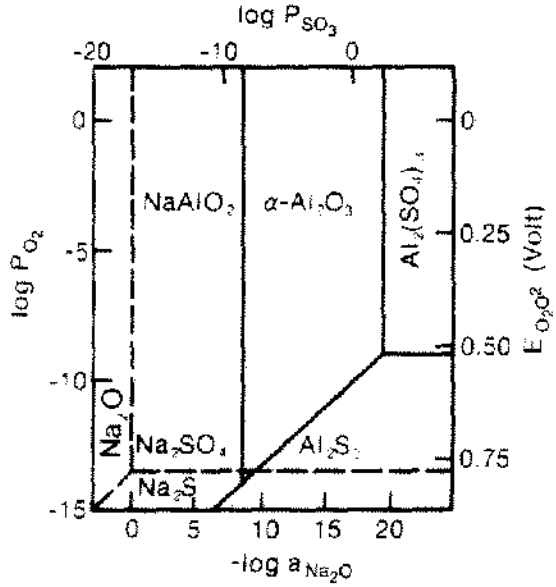

Figure 8. Phase Stablity Diagram for Al_2O_3 in Na_2SO_4 at 1200 K from Rapp (1980).

Molten Carbonates and Hydroxide Fluids

Two of the candidate heat-transfer and storage fluids that show promise for operation at 900°C are carbonates and hydroxides. We used a eutectic mixture (Janz et al., 1979) of reagent grade Na_2CO_3 and reagent grade K_2CO_3 that contained 58 mol % (51.5 wt %) of Na_2CO_3 to evaluate the compatibility of materials in carbonates at 900°C. The molten carbonate was purged during the experiment with dry nitrogen containing 20 ppm of CO_2; a flow rate of 50 cc/min was used.

We used thermochemical data (Anderson, 1975) on the activity coefficient (Klotz, 1964) for the oxide in the reaction,

$$(Na,K)_2CO_3(\ell) \rightleftharpoons (Na,K)_2O(\ell) + CO_2(g),$$

where the alkali liquids are of eutectic composition to calculate the mole fraction of the oxide in the melt at equilibrium with 20 ppm CO_2. We found it to be 10^{-2}; however, for the experiments done in this work we estimated that the actual mole fraction was about 10^{-3} since the purge rate for removing the CO_2 was only 50 cc/min and the time for the experiment was about 50 hours.

We used reagent grade NaOH at 900°C for the hydroxide screening tests. The molten hydroxide was purged at 50 cc/min with nitrogen containing about 1 ppm H_2O. Activity coefficient information on the decomposition reaction

$$2NaOH(\ell) \rightleftharpoons Na_2O(\ell) + H_2O(g)$$

was not available as for the carbonate salt so we could not calculate the equilibrium concentration of Na_2O. However, estimates of the H_2O partial pressure from the thermochemical data (Stull and Prophet, 1971) along with the information on purge rate and time of the experiment (80 hours) indicated that the mole fraction of Na_2O in NaOH would be about 1%. This is 10 times higher than in the carbonate and indicates that NaOH molten salt is more basic than the carbonate under the conditions used for these experiments.

For both the carbonate and hydroxide, free moisture was removed from the salts before they were melted by heating in a vacuum oven at 100°C for 16 hours.

Corrosion Tests

The corrosion screening tests on candidate molten salt containment materials consisted of submerging test coupons in the molten salt at 900°C for a period of 50 to 100 hours. About 16 coupons were tested simultaneously in a crucible. The weight of each coupon and its thickness was measured before and after exposure to the molten salt. The purpose of these tests was to identify the most promising types of materials for containing molten salts and to rank the candidate fluids for corrosiveness.

The results of the studies are shown in Tables 1, 2 and 3, where the type of material is indicated as well as its chemical composition. The loss by corrosion from the coupons is given in μm/day per exposed side along with the exposure time in hours, which is given in parentheses. Most of the corrosion rate data were derived from the weight change information for the coupon; however, for some coupons that fractured during testing, the thickness change was used. Weight losses were converted to thickness losses in

TABLE 1

Apparent Corrosion Rate for Alloys in Molten Salts at 900°C

Material	Composition	Apparent Corrosion Rate (μm/day)*		Comments
		Carbonate	Hydroxide	
Inconel 600	74 Ni/15.5 Cr/8 Fe	5(50)	10(84)	
Cabot 600	74 Ni/15.5 Cr/8 Fe	5(50)	−16(84)	
Incoloy 800	43 Fe/32.5 Ni/21 Cr	13(50)	−24(84)	
Cabot 800H	43 Fe/32.5 Ni/21 Cr	10(50)	−32(84)	
Inconel X750	73 Ni/15.5 Cr/7 Fe/2.5 Ti	1(50)	−13(84)	
Stainless 304	68 Fe/19 Cr/10 Ni/2 Mn	15(50)	d(84)	
Stainless 316	67 Fe/17 Cr/11 Ni/2 Mo/2 Mn	10(50)	d(84)	
Nickel	99.99 + Ni	10(50)	18.3(84)	Showed gain boundary etching in hydroxide.
Haynes 230	56 Ni/22 Cr/14W/2 Fe/2 Co/2 Mo	−10(50)	d(84)	
Haynes 556	32 Fe/21 Cr/20 Ni/20 Co/3 Mo/3 W	5(50)	−47(84)	
Cabot 214	75 Ni/16 Cr/4.5 Al/4 Fe	11(50)	−66(84)	
Haynes 188	38 Co/22 Ni/22 Cr/14 W/3 Fe	14(50)	d(84)	
Cabot R-41	52 Ni/19 Cr/11 Co/10 Mo/5 Fe/1.5 Al/3 Ti	3(50)	d(84)	
Hastelloy S	64 Ni/16 Cr/15 Mo/3 Fe/2 Co	8(50)	−2(84)	
Hastelloy N	71 Ni/17 Mo/7 Cr/5 Fe	10(50)	d(84)	
Hastelloy X	48 Ni/22 Cr/18.5 Fe/9 Mo/1.5 Co	−2(50)	−8(84)	

*Exposure time in hours is in parentheses; d indicates the coupon disintegrated. Apparent corrosion rates with superscript 1 are determined by thickness change; the rest are determined by weight. Negative corrosion rates indicate a weight gain.

TABLE 2

Apparent Corrosion Rates for Fused-Cast and Dense Al_2O_3 Ceramics in Molten Salts at 900°C

Material	Composition	Apparent Corrosion Rate (μm/day)* Carbonate	Hydroxide	Comments
Window	Sapphire	0 (48)	11 (92)[1]	Single crystal clouded after carbonate and hydroxide exposure
	$Mg Al_2O_4$	1 (48)[1]	...	Polycrystalline, translucent after carbonate exposure
Fused-Cast	99.3 Al_2O_3	40 (40)	60 (65)[1]	Slightly friable
	94.5 Al_2O_3/3.9 Na_2O/1 SiO_2	−12 (40)	d (65)	Increased thickness in carbonate, slightly friable
	93.9 Al_2O_3/5.6 Na_2O	−10 (48)	d (65)	Increased thickness in carbonate
	78 Cr_2O_3/8.7 MgO/7.9 Fe_2O_3/4 Al_2O_3/1.6 SiO_2	110 (40)	d (65)	
	60 Al_2O_3/27 Cr_2O_3/6 MgO/4 Fe_2O_3/2 SiO_2	20 (40)	45 (92)[1]	
	50 Al_2O_3/36 ZrO_2/12 SiO_2	30 (40)	d (65)	Increased thickness in carbonate
	$MgO \cdot Al_2O_3$(72 Al_2O_3)	16 (40)	d (92)	
	Eutectic $MgO \cdot Al_2O_3$(55 Al_2O_3)	13 (48)	30 (65)[1]	
Dense alumina	99.8 Al_2O_3	1 (48)	110 (65)[1]	Orange peel surface in hydroxide
	99.5 Al_2O_3	2.5 (40)	110 (65)[1]	**
	99.0 Al_2O_3	1 (48)	...	**
	96 Al_2O_3	31 (60)	d (65)	**
	96 Al_2O_3	25 (60)	60 (65)[1]	**
	95 Al_2O_3	25 (60)	d (92)	**

*Exposure time in hours is in parentheses; d indicates the coupon disintegrated. Corrosion rates with superscript 1 are determined by thickness change; the rest are determined by weight. Negative corrosion rates indicate a weight gain.

**All dense Al_2O_3 coupons lost thickness after exposure to the carbonate salt.

TABLE 3

Apparent Corrosion Rates for Ceramics in Molten Salts at 900°C

Material	Composition	Apparent Corrosion Rate (μm/day)* Carbonate	Hydroxide	Comments
Dense alumina	94 Al_2O_3	16 (60)	d (92)	**
	91 Al_2O_3	29 (60)	d (65)	**
	90 Al_2O_3	30 (60)	d (92)	**
	86 Al_2O_3	29 (60)	d (92)	**
	85 Al_2O_3	42 (60)	d (65)	**
Porous ZrO_2	Y_2O_3 stabilized	−18 (48)	d (92)	8% closed pores, increased thickness in carbonate
Porous ZrO_2	MgO stabilized	−16 (48)	d (92)	8% closed pores, increased thickness in carbonate
Porous MgO	99.5 MgO	−100 (48)	100 (65)[1]	17% pores***
Refractory	98.2 MgO/1 CaO/0.5 SiO_2	50 (28)	d (92)	17% pores***
Refractory	61.5 MgO/17.3 Cr_2O_3/11 Fe_2O_3/8 Al_2O_3	50 (28)	d (92)	14% pores***
Refractory	Super duty fireclay, premium	−150 (48)	d (92)	11% pores***
Refractory	Super duty fireclay	−60 (28)	d (65)	10% pores***
Refractory	99.2 Al_2O_3/0.4 SiO_2	30 (28)	d (92)	20% pores***
Refractory	71.2 Al_2O_3/25 SiO_2/2.8 TiO_2/1 Fe_2O_3	d (28)	...	16% pores***
Refractory	36 MgO/25 Cr_2O_3/22 Al_2O_3/12 Fe_2O_3	150 (28)	...	20% pores ***
Refractory	66 ZrO_2/32 SiO_2/1 Al_2O_3	−60 (28)	d (92)	22% pores****

*Exposure time in hours is in parentheses; d indicates the coupon disintegrated. Corrosion rates with superscript 1 are determined by thickness change; the rest are determined by weight. Negative corrosion rates indicate weight gain.

**All dense Al_2O_3 coupons lost thickness after exposure to the carbonate salt.

***All refractories were friable after exposure to the carbonate salt.

the tables by using the bulk density of the coupon. A positive corrosion rate indicates a loss of weight while a negative value indicates a gain in weight.

Corrosion Results for Alloys

Many of the alloys completely disintegrated in the hydroxide at 900°C after 84 hours (Table 1). The remaining coupons from the hydroxide experiments all showed evidence of extensive corrosion. For instance, alloy 214 in hydroxide showed a blackened surface, cracking along the edge of the coupon, and flaking of the corrosion product. A protective oxide coating did not form. This cracking of the coupon or flaking of the oxide layer occurred with all alloy coupons tested in both hydroxide and carbonate. The alloy 214 in carbonate molten salt did not crack, but the oxide layer flaked. The damage was generally less severe in the carbonate than in the hydroxide.

The corrosion rate values reported in the table for these alloys were all derived from weight loss information and most of the results indicated a gain in weight for the coupon (in these studies the corrosion product was not removed prior to weighing and measuring the coupon). Additionally, the thickness measurements indicated a gain in thickness for all of the alloys after exposure to both hydroxide and carbonate molten salts. For the alloys with thick oxide scales the weight gain was caused by oxidation of the alloy, and the thickness gain was probably caused by the porous nature of the oxide scale. For some coupons, for instance 99.99 + % Ni in hydroxide, there was no evidence of scale, but the coupon had gained in thickness despite weight loss. This swelling of the coupon may result from dissolution of Na metal from the melt or formation of a high volume grain boundary phase. The seemingly low corrosion rates in Table 1 mask the fact that metal was being lost from the alloys and converted to scale.

For all of the alloys evaluated it appeared that in hydroxide and carbonate molten salts the alloys readily corroded without forming a protective coating and would not be expected to exhibit long life. This rapid oxidation rate occurred despite making both melts low in oxidation potential by excluding oxygen in the atmosphere above the melt and by maintaining low partial pressures of CO_2 and H_2O in the respective melts. To further lower the oxidation potential would require using hydrogen in the gas above a hydroxide melt, which reportedly results in low corrosion rates for Ni (Smith, 1956).

Corrosion Results for Ceramics

The corrosion results for a number of ceramic materials at 900°C are shown in Tables 2 and 3 (as with the alloys, the corrosion product was not removed prior to weighing and measuring; however, it appeared to be very thin). The sapphire window material exhibited the best corrosion resistance of the materials tested for both the carbonate and hydroxide molten salts, showing no detectable corrosion rate for the former and an 11 μm/day corrosion rate for the latter. Figure 9 shows one of the sapphire window coupons before testing and after exposure to carbonate molten salt (note that the coupon fractured during testing) where a white deposit formed on the sapphire; a similar deposit was seen after exposure to the hydroxide melt. We think that this deposit is a protection layer of sodium aluminate ($NaAlO_2$), which has been reported to protect Al_2O_3 from corrosion in carbonate melts (Grantham and Terry, 1976). Figure 10 illustrates what we think is the mechanism that protects sapphire and other high purity Al_2O_3 ceramics. The Al_2O_3 reacts with Na^+ in the melt to cover the surface with an insoluble layer of $NaAlO_2$. The $MgAl_2O_4$ spinel window material also showed a very low corrosion rate in the carbonate but was not tested in the hydroxide.

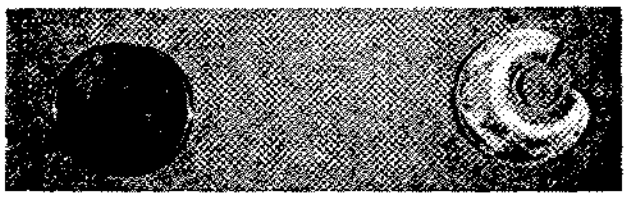

Figure 9. Sapphire before and after Exposure to Carbonate at 900°C for 48 Hours—Coupon Fractured, Top Right, in the Carbonate.

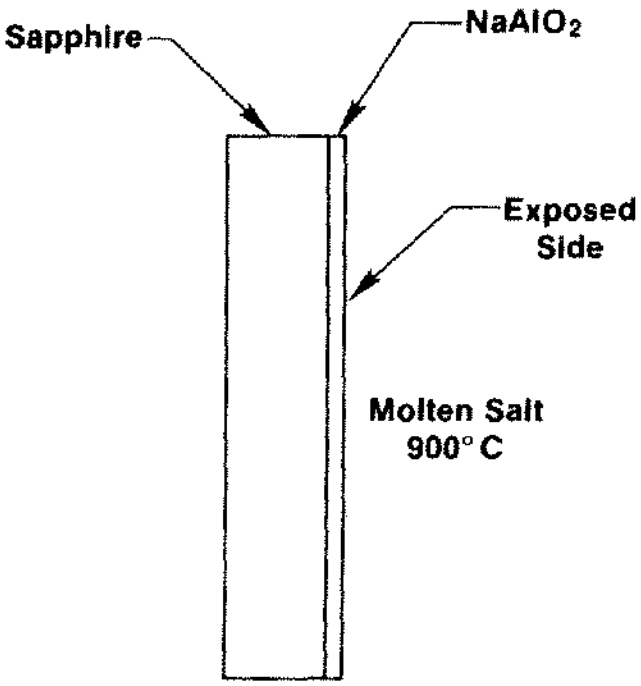

Figure 10. Illustration of the Corrosion of High Purity Al_2O_3 in Na^+ Containing Molten Salt.

In agreement with the results on the window materials, the high Al_2O_3 and the eutectic $MgO \cdot Al_2O_3$ fused-cast materials in Table 3 had low corrosion rates in both salts. Another fused-cast material that performed well in both molten salts was the 60 Al_2O_3/27Cr_2O_3. Two of the high alumina fused-cast materials showed increased weight—indicated by a negative corrosion rate—after exposure to carbonate, as seen in Table 2, and showed increased thickness as well. Additionally, the fused-cast material with 36% ZrO_2 (Table 2) as well as the three materials in Table 3 that contain ZrO_2 all showed thickness increases. The reason for the swelling of these coupons is not presently clear; however, it may indicate an attack by the salt at grain boundaries.

Another type of material that resisted corrosion well in both salts was the high-purity, dense Al_2O_3 materials. The best of these materials, as seen in Table 2, appear to resist corrosion very well in the carbonate but not as well in the hydroxide. Figure 7 shows 99.8% Al_2O_3 before testing and after testing in hydroxide. Corrosion pits are seen on the surface after the hydroxide exposure; however, the same material in carbonate is virtually untouched (it looked the same as the untested material seen in the figure). Figure 11 illustrates the influence of corrosion in these high density Al_2O_3 materials. The grains of Al_2O_3 are represented by large and small circles bonded together with a glass such as $CaO \cdot SiO_2$. Increased amounts of glass phase are commonly found in the grain boundaries of oxide materials as the purity of the material decreases. The molten salt readily attacks the glass (Grantham and Ferry, 1976; Janz and Tompkins, 1979), which tends to loosen and remove the smaller particles, leading to a rougher appearance under a microscope and a rougher feel to the coupon.

Another material that resisted corrosion well in both salts was MgO. As seen in Table 3, this material had 17% porosity and after carbonate exposure showed a weight gain, probably caused by the salt trapped in its pores, and a gain in thickness.

The refractory materials in Table 3 were porous, showed friability after carbonate exposure and disintegrated after hydroxide exposure. Figure 12 shows a refractory material before and after exposure to molten carbonate. The material has crumbled along the edges after exposure, has become lighter in color and the large grains are more in evidence than before testing, which indicates that the small grains have fallen away. Figure 13 illustrates how molten salt has access to the interior of such a sample through the pores and can readily loosen larger pieces of material by attacking the silicate bonding material inside the sample as well as on the surface, as with the dense Al_2O_3 materials.

The carbonate corrosion results for ceramics shown in Tables 2 and 3 indicate that several fused-cast materials, the high purity window materials, several dense Al_2O_3 materials, ZrO_2 and MgO are all promising candidates for use in contact with the molten carbonates. The results for the hydroxide salt indicates that some of the fused-cast materials and the sapphire window material are the most promising.

Comparison of Carbonate and Hydroxide Molten Salts

A comparison of the corrosion results in the tables for the carbonate and the hydroxide indicates that the hydroxide

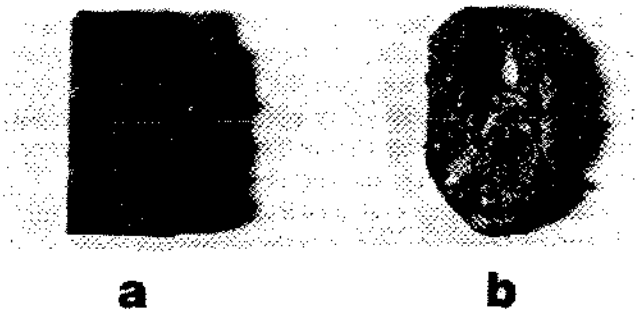

Figure 12. Refractory Brick before and after Carbonate at 900°C for 28 Hours.

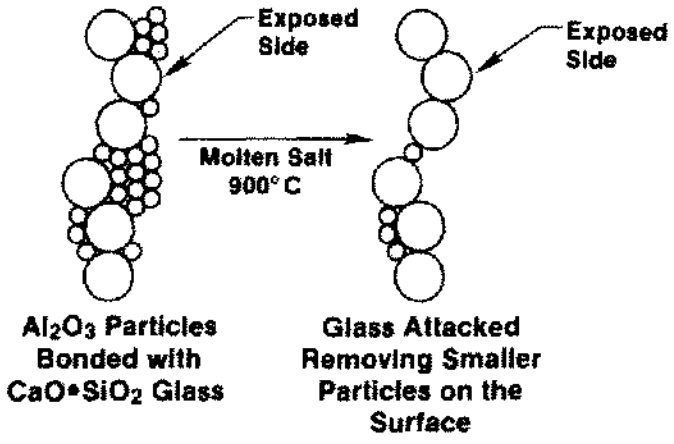

Figure 11. Illustration of the Influence of the Grain Boundary Bonding Phase on the Corrosion of Ceramics.

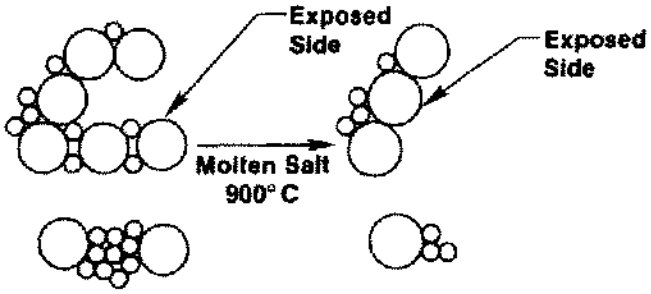

Figure 13. Illustration of the Influence of Open Pores on the Corrosion of Ceramics.

is about 3 to 10 times more corrosive toward alloys and ceramics. However, as discussed earlier, the corrosiveness generally depends on the chemistry of the salt. Thus, results for a range of CO_2 and H_2O partial pressures for the carbonate and hydroxide, respectively, need to be done to more fully explore the corrosiveness of these salts. Under the conditions in this work there was 10 times more sodium oxide in the hydroxide than in the carbonate, which may explain the greater corrosiveness of the hydroxide.

SUMMARY AND CONCLUSIONS

This paper presented the applications for high-temperature molten salts as well as the chemical character of molten salts as applied to corrosion. We also presented the results of experiments on the corrosion of materials in molten eutectic Na_2CO_3/K_2CO_3 and in molten NaOH at 900°C. The coupon exposure time in the carbonate salt was about 50 hours, while in the hydroxide salt it was about 80 hours.

We found the high-purity aluminum oxide, magnesium oxide, zirconium oxide and magnesium aluminate to be the most corrosion resistant along with several types of fused-cast refractories.

The corrosion results suggested that increased glass phase leads to lower corrosion resistance. Increased amounts of glass phase are commonly found in the grain boundaries of oxide materials as the purity of the material decreases. Refractories also contain relatively large amounts of glass phase.

Higher porosity of the material also leads to decreased corrosion resistance because the molten salt has better access to the interior of the material. Open porosity, as exhibited by the refractory materials, coupled with large amounts of glass phase appears to lead to very low corrosion resistance, as the results on the refractory materials indicate.

We observed in these experiments that alloys developed an oxide scale that continually spalled. Thus, the amount of metal phase was continually decreasing while the alloy was being exposed to these salts.

These results indicated that the hydroxide molten salt was more corrosive to both alloys and ceramics than carbonate molten salt at 900°C. Under the conditions used in these experiments, estimates of the oxide ion content for the salts indicated that the hydroxide had 10 times more oxide ion than the carbonate. This higher oxide ion content makes the hydroxide melt more basic, which may explain the higher corrosion rates in the hydroxide.

ACKNOWLEDGMENTS

We acknowledge the support of J. Dolan for constructing the apparatus and M. Guiterrez for preparing some of the coupons. We are indebted to T. Thomas for helpful discussions. We acknowledge the U.S. Department of Energy Thermal Storage Program for support in initiating this work and assembling the first corrosion furance and their continuing support in conducting corrosion studies. We also acknowledge the support from the U.S. Department of Energy Solar Thermal Program that allowed us to expand the effort to include more candidate materials. This work was supported by the U.S. Department of Energy under contract no. EG-77-C-01-4042.

REFERENCES

Andersen, B. K. 1975. *Thermodynamic Properties of Molten Alkali Carbonates*, PhD Thesis from Tech. Univ. of Denmark.

Battleson, K. W. et al. 1980. *1980 Solar Central Receiver Technology Evaluation*, SAND/80-8235, Sandia National Laboratories, Livermore, CA, May.

Brumleve, T. D. 1978. "Status Report on the Direct Absorption Receiver," presented at the Advanced Solar Thermal Technology Semiannual Review, May 9–11, SAND/78-8702, Sandia National Laboratories.

Copeland, R. J., J. W. Leach and C. Stern. 1982. "High-Temperature Molten Salt Solar Thermal Systems," *Proceedings of 15th Intersociety Energy Conversion Engineering Conference*, Los Angeles, CA, Aug. pp. 2032–2030.

Copeland, Robert J. 1982. "Advanced, High-Temperature Molten Salt Storage," Presented at the Energy Storage Contractors' Review Meeting.

Flood, H., T. Forland and K. Motzfeld. 1952. *Acta Chem. Scand.* Vol. 6, p. 257.

Foreman, R. W. 1980. "Heat-Treatment of Industrial Materials in Molten Salt," *Proceedings of the Third International Symposium on Molten Salts*, 158th Electrochemical Soc. Mtg., Hollywood, FL, October 8.

Grantham, L. F. and P. B. Ferry. 1976. "Corrosion in Alkali Metal Carbonate-Based Melts" *Proceedings of the International Symposium on Fused Salts*, Edited by J. D. Pemsler, Electrochemical Society, Inc., Princeton, NJ.

Ingram, M. D. and G. J. Janz. 1965. "The Thermodynamics of Corrosion in Molten Carbonates: Application of E/pCO_2 Diagrams," *Electrochimica Acta 10*, Vol. 783.

Inman, D. and N. S. Wrench. 1966. Corrosion in Fused Salts, *Brit. Corros. J.*, Vol. 1, p. 246.

Janz, G. J. and R. P. T. Tompkins. 1979. *Corrosion in Molten Salts: An Annotated Bibliography*, NACE Vol. 35, p. 485.

Janz, G. J., et al. 1979. *Physical Properties Data Compilations Relevant to Energy Storage*, NSRDS-NBS 61 Part II, U.S. Depart. of Commerce, Washington, D.C.

Klotz, I. 1964. *Chemical Thermodynamics*, W. A. Benjamin, Inc., New York.

Littlewood, R. 1962. "Diagrammatic Representation of the Thermodynamics of Metal-Fused Chloride Systems," *J. Electrochem. Soc.* Vol. 109, No. 6, p. 525.

Lux, H. 1939. *Z. Elektrochem.*, Vol. 45, p. 303.

Mar, R. W. and R. W. Carling. 1980. "The Application of Molten Salts to Solar Large Power Systems," *Proceedings of the Third International Symposium on Molten Salts*, Edited by G. Mamantoy, M. Blander and G. P. Smith, The Electrochemical Society, Volume 81-9, Pennington, NJ.

Rapp, R. R. and K. S. Goto. 1980. "The Hot Corrosion of Metals by Molten Salts," *Proceedings of the Second International Symposium on Molten Salts*, Edited by J. Braunstein and J. R. Selman, The Electrochemical Society, Volume 81-10, Pennington, NJ, p. 159.

Smith, G. P. 1956. "Corrosion of Materials in Fused Hydroxides," *Nuclear Metallurgy*, Amer. Inst. Mining Metal Engrs., Inst. Metals Div., pp. 71-94.

Stull, D. R. and H. Prophet. 1971. *JANAF Thermochemical Tables*, 2nd Edition, NSRDS-NBS37 U.S. Department of Commerce, Washington, DC.

Tallerico, T. N. 1979. *A Description and Assessment of Large Solar Power Systems Technology*, SAND79-8015, Sandia National Laboratories, August.

Watt, B. W. and D. H. Kerridge. 1979. *Chem. in Britain*, Vol. 15, p. 78.